

# Getting the electrons right for O2-on-metal systems Bree, R.A.B. van

#### Citation

Bree, R. A. B. van. (2025, October 21). *Getting the electrons right for O2-on-metal systems*. Retrieved from https://hdl.handle.net/1887/4279459

Version: Publisher's Version

Licence agreement concerning inclusion of doctoral

License: thesis in the Institutional Repository of the University of

<u>Leiden</u>

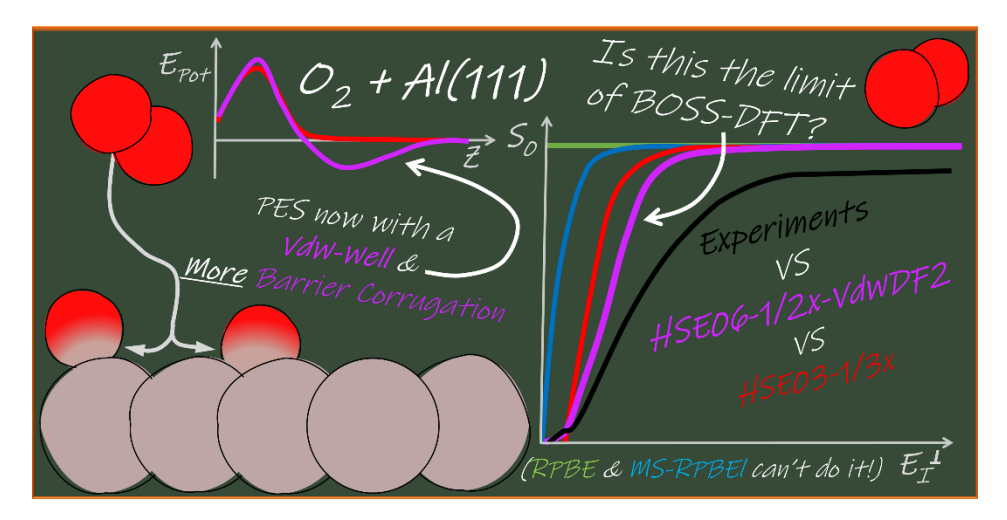
Downloaded from: <a href="https://hdl.handle.net/1887/4279459">https://hdl.handle.net/1887/4279459</a>

**Note:** To cite this publication please use the final published version (if applicable).

## 4 Limits of BOSS DFT: O<sub>2</sub> + Al(111) dynamics on a screened hybrid Van der Waals DFT potential energy surface

#### This chapter is based on:

van Bree, R. A. B.; Kroes, G. J. Limits of BOSS DFT: O<sub>2</sub> + Al(111) Dynamics on a Screened Hybrid Van der Waals DFT Potential Energy Surface. *J. Phys. Chem. C* **2025**, *129* (11), 5408–5421. https://doi.org/10.1021/acs.jpcc.5c00327.



## **Abstract**

The activated dissociative chemisorption (DC) of  $O_2$  on Al(111) is a thoroughly studied benchmark system for oxygen–metal interactions. However, research based on density functional theory (DFT) has not yet been able to accurately determine the electronic structure, and theory as a whole has so far been unable to reproduce measured sticking probabilities with chemical accuracy. Previous work has argued that this is likely due to the inability of DFT at the generalised gradient approximation (GGA) level to describe the barriers to DC of  $O_2$  on Al(111) correctly. The argument is that the most commonly applied electronic structure approach in surface science, which involves the use of GGA-DFT, yields too low reaction barriers for the DC of  $O_2$  on Al(111). Moreover, it seems that GGAs will generally fail to accurately predict barriers for systems with low charge transfer energy, i.e., systems for which charge transfer from metal to molecule

at the transition state is likely. Subsequent work on both  $O_2$  + Al(111), i.e., Chapter 3, and O<sub>2</sub> + Cu(111), i.e., Chapter 5, has suggested that screened hybrid density functionals (DF) yield more accurate barrier heights for DC on metal surfaces. However, so far the use of only a screened hybrid DF was not enough to ensure a highly accurate description for O<sub>2</sub> + Al(111). Even though the onset of the sticking probability  $(S_0)$  curve was correctly described, the slope, or width, of the curve was not. The use of a non-local correlation DF combined with an increased fraction of exact exchange in the screened hybrid exchange DF was believed to further improve the description of the electronic structure by increasing the energetic corrugation of the barrier. This approach was assumed to increase the width of the sticking curve without lowering the incidence energy for the reaction onset, thus reducing the slope of the sticking curve. To test this, we present quasi-classical trajectory (QCT) calculations on the  $O_2$  + Al(111) system based on a potential energy surface (PES) computed with the HSE06-1/2x-VdWDF2 screened hybrid Van der Waals DF, using the Born-Oppenheimer static surface (BOSS) model. The resulting PES shows the presence of shallow Van der Waals wells in the entrance channel. Furthermore, the barriers to DC show a slightly higher energetic corrugation than the previously used HSE03-1/3x screened hybrid DF, although most differences are smaller than 1 kcal/mol. These minor alterations in the PES with respect to previous work mean that the  $S_0$  computed for  $O_2$  + Al(111) using the HSE06-1/2x-VdWDF2 DF are somewhat improved over the previous results. Specifically, the onset of the  $S_0$  curve is now somewhat better described and the curve is broadened a little compared to the HSE03-1/3x description. These results, in combination with previous studies, imply that future electronic structure methods would need to provide larger changes in the PES, or a different dynamical model would need to be used to bring theory in better agreement with the experiment. Moreover, future higherlevel theory also needs to address the currently very demanding computational costs of screened hybrid plane-wave-DFT for molecule-metal interactions.

#### 4.1 Introduction

The rate of heterogeneously catalysed processes is often controlled by the dissociative chemisorption (DC) of a molecule on the active centre of the catalyst  $^{6,212,213}$ . Furthermore, for oxidative catalysis or oxide formation, the DC of  $O_2$  is often the first and most critical step $^{214-216,218}$ . The key interactions that are at play in the DC of  $O_2$  on metals are not yet fully understood  $^{124,229,231}$  and are therefore of substantial scientific interest  $^{1,55,56,219}$ . The  $O_2$  + Al(111) system has over the years become a benchmark for the DC of  $O_2$  on metal systems  $^{214,222-227}$ . However, unlike the perhaps better-known  $H_2$  + Cu(111) benchmark system  $^{55,110,135}$ , theoretical models are not yet able to describe the DC of  $O_2$  on Al within chemical accuracy  $^{124}$ , nor is there a clear scientific consensus on the origins of the barrier to DC for this system  $^{228-235}$ .

Both the failure of theoretical models to describe the DC of  $O_2$  on Al(111) and the ongoing discussion on the origin of the barrier to reaction can be related to the inability of the most commonly applied density functional theory (DFT) method in surface science to compute the DC barrier<sup>124,228,240,229–231,234–238</sup>. The generalised gradient approximation (GGA) approach to the density functional (DF) remains the most commonly used approach to compute reaction barriers<sup>56</sup> within surface science because it represents a good compromise between accuracy and computational costs. However, recent work<sup>124</sup> strongly suggests that the GGA approach will fail to compute accurate reaction barriers if the charge transfer energy ( $E_{CT}$ ) is below T eV, where  $E_{CT}$  is defined as:

$$E_{CT} = \phi - EA \tag{4.1}.$$

Here  $\phi$  is the work function of the metal surface, and EA is the electron affinity of the molecule reacting on that surface<sup>124</sup>. If  $E_{CT}$  is below  $7\,eV$  even one of the most "repulsive" (i.e., a "more repulsive DF" is a DF generally predicting higher DC barriers) GGA DFs (i.e., RPBE<sup>239</sup>) tends to underestimate the barrier height to DC<sup>55,56,129,161</sup>. This means that, when constructing a chemically accurate semi-empirical DF using the specific reaction parameter approach, i.e., an SRP DF, basing this DF on GGA DFs will probably not be possible<sup>124,129</sup>. For O<sub>2</sub> + Al(111)  $E_{CT} = 3.8\,eV^{124}$ , and all GGA DFs fail to compute any relevant barrier. This in turn results in computed reaction probabilities that are always equal or close to one and thereby in disagreement with the experiment, which shows activated

dissociation for  $O_2$  on Al(111)<sup>124,236–238</sup>. Likewise, meta-GGA DFs, which are on the next rung up on Jacob's ladder<sup>279</sup>, show only a minor improvement over GGA results for  $O_2$  + Al(111)<sup>124</sup>.

At this time it is not fully understood why  $E_{CT} < 7 \text{ eV}$  results in a failure of DFs containing semi-local exchange for DC on metals. The failure of GGA DFs to accurately predict barriers for molecule-metal reactions may be related to the more general failure of GGA DFs to predict barriers for gas-phase reactions, as also previously discussed by Gerrits et al. 124. The commonly applied reasoning is that GGA DFs favour the delocalised nature of a transition state (TS) and thus result in TS-energies that are too low compared to the reactants, resulting in too low or even eliminating the barriers. For gas-phase reactions such a "densitydriven" error could then be and has been resolved by using semi-local DFs in a non-self-consistent-field (NSCF) manner by applying a GGA-DF once to a converged density obtained with a hybrid DF, i.e., a "HF-based density", where HF stands for Hartree-Fock<sup>147–149,253</sup>. However, the explanation that this approach yields more accurate barriers due to correcting for density-driven errors has come under scrutiny as recent work indicates that the improved agreement is due to a cancellation between both density-driven and "functional-driven" errors 150,151. Moreover, the explanation in terms of only density-driven errors is also at odds with previous results from Chapter 3 for O<sub>2</sub> + Al(111), which showed that good sticking probabilities can be computed with both SCF- and NSCFscreened hybrid approaches, where in the latter a screened hybrid DF is applied just once to a converged GGA density. This implies that the greater part of the GGA-DFT error for  $O_2$  + Al(111) should be functional-driven <sup>147,253,280</sup>, see also Chapter 3.

Regardless of the origin of the error of the semi-local exchange DF, previous work suggests that the failure of these types of DFs for  $O_2$  + Al(111) should be avoided by employing a screened hybrid DF instead<sup>124,280</sup>. The use of the screened hybrid HSE03-1/3x DF resulted in reaction probabilities that were in semi-quantitative agreement with the experiments. Especially the reaction probabilities at lower normal incidence energy ( $E_i^{\perp}$ ) closely reproduce experimental results<sup>124,145,280</sup>. However, at higher  $E_i^{\perp}$  the computed sticking probabilities still overestimate the experimentally determined sticking probabilities. This resulted in a reaction

probability curve that is too steep, or too narrow<sup>124,280</sup>, as also seen in Chapter 3. To find a DF that can reproduce experiments with chemical accuracy for systems like  $O_2 + Al(111)$ , this problem still needs to be fixed.

Several alternative possibilities could contribute to a too-narrow reaction probability curve. The first few are due to the use of the Born-Oppenheimer static surface (BOSS) model. In the Born-Oppenheimer approximation, the electronic energy is decoupled from nuclear motion, and in the static surface approximation, the surface atoms of the metal are kept fixed in their ideal surface lattice positions. Because experiments indicate a limited influence of surface temperature on the reaction probability of  $O_2$  on Al(111)<sup>224</sup>, it is not immediately expected that the inclusion of surface phonon motion will substantially influence the reactivity 124,224,280. Furthermore, if the barrier location as described by the HSE03-1/3x DF is to be taken as accurate, which is likely according to previous work<sup>129</sup>, then the O<sub>2</sub> + Al(111) system will generally have "early" barriers, i.e., the barriers will be located at large molecule-surface distances<sup>124,145,228–230,280</sup>. Such early barriers tend to limit the effects of energy dissipation from the motion of the molecule to surface atom motion<sup>124,274,275</sup>. Furthermore, the early barrier and the high mass of O<sub>2</sub> also suggest that the effects of electron-hole pair (ehp) excitation, which can be described with electronic friction approaches, should be small<sup>162,170,281</sup>. This likely also eliminates the effects of ehp excitation as a possible important cause for the disagreement between theory and experiments for  $O_2 + Al(111)$ .

If we assume that the BOSS model is not to blame for the currently deficient theoretical description of the DC of  $O_2$  on Al(111), only the electronic structure description remains a likely cause of error, as also previously argued in Chapter 3 and Refs. <sup>124,280</sup>. As stated above it was expected that the inclusion of longrange Van der Waals (VdW) correlation in the exchange-correlation functional could result in a broadening of the reaction probability curve, but this has so far not yet been corroborated. This hypothesis is supported by the argument that the introduction of a VdW well will increase both the energetic and geometric corrugation of the barrier sight varies with the impact point of the surface and the orientation of the molecule and this strongly influences the width of the reaction probability

curve<sup>161,254</sup>. Additionally, a VdW well could alter the dynamics of O<sub>2</sub> impinging on the surface by accelerating the molecule towards the metal surface before dissociation<sup>132</sup>.

In this chapter, we aim to investigate the simultaneous effects of the inclusion of VdW correlation and of admixing a larger amount of exact exchange on the potential energy surface (PES) as well as the dynamics of the DC of O<sub>2</sub> on Al(111), by computing and analysing a PES based on the HSE06-1/2x-VdWDF2 DF and comparing quasi-classical trajectory (QCT) dynamics results based on this PES to experiments and previous theoretical studies. The aim of applying this DF is to hopefully resolve the current shortcomings in the description of the DC of O<sub>2</sub> + Al(111). This chapter is set up as follows: Section 4.2.1 will discuss the details of the DF used to compute the electronic structure, Section 4.2.2 the computational details of the DFT calculations, Section 4.2.3 the Al(111) lattice details, Section 4.2.4 the PES fitting technique, and Section 4.2.5 the QCT calculations. Thereafter, the DFT results are shown in Section 4.3.1, and in Section 4.3.2 the QCT dynamics results are shown. Section 4.3.3 then discusses the results in the context of previous work and presents an outlook for future work. The chapter is summarised and conclusions are provided in Section 4.4. Lastly, the appendixes to the chapter are presented in Section 4.5.

## 4.2 Methods

In this chapter, the Born-Oppenheimer static surface (BOSS) model is employed  $^{56}$ . In short, this signifies that the motion of the nuclei is decoupled from the motion of the electron via the Born-Oppenheimer approximation, and that the Al surface atoms are kept static in their ideal (111) surface lattice positions. As a result, the dynamics of the  $O_2$  on the Al(111) system only requires a description of the motion in the remaining six molecular degrees of freedom. These six degrees of freedom in addition to a description of the high symmetry sites on the Al(111) surface are shown in **Figure 4.1** and discussed in greater detail in other work  $^{55,124,280}$ , see also Chapter 3.

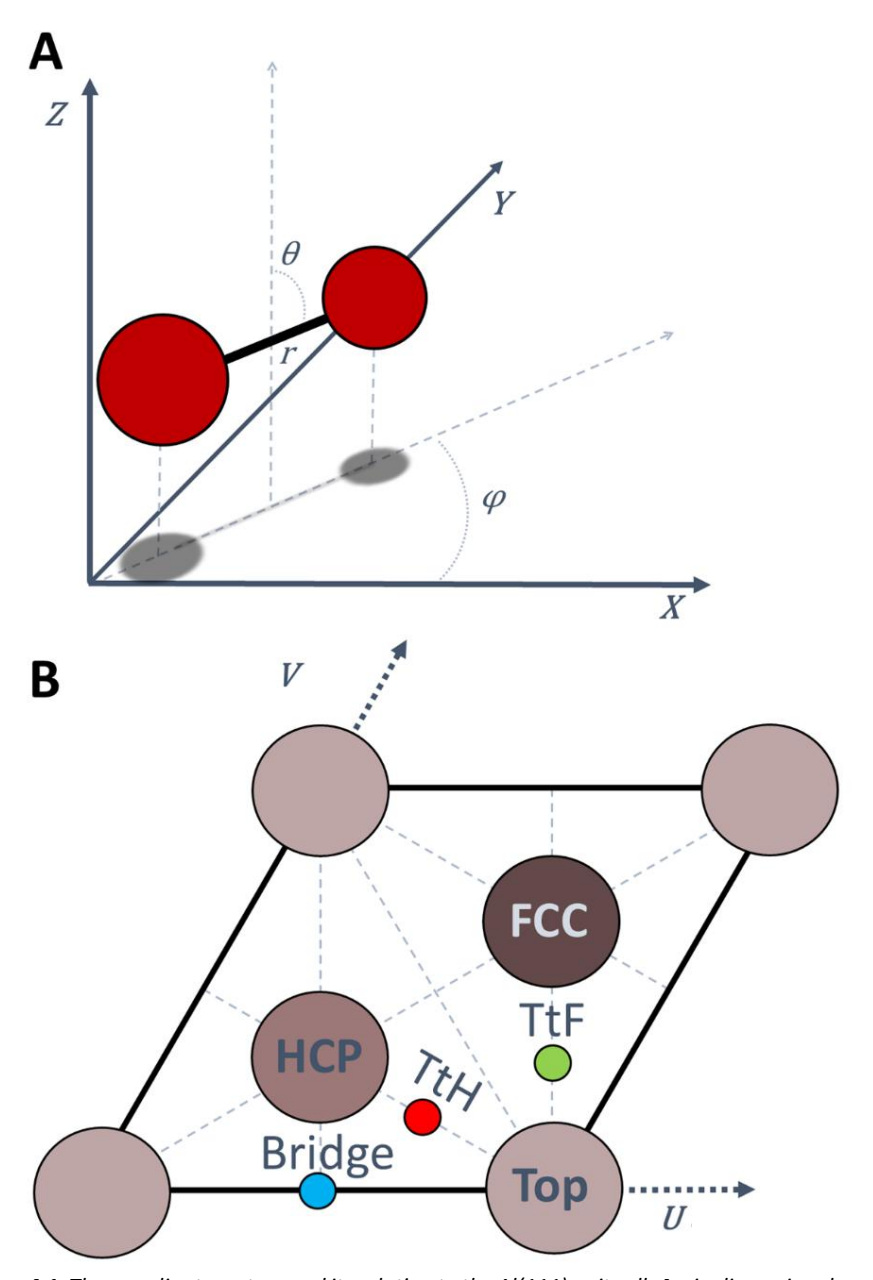


**Figure 4.1**: The coordinate system and its relation to the Al(111) unit cell; **A**: six-dimensional centre-of-mass coordinate system for the  $O_2$  molecule; **B**: (111) surface unit cell for an FCC metal (Al) with all high symmetry sites indicated. A darker shade represents an atom that is in a deeper layer in the slab.

#### 4.2.1 Electronic structure

For this chapter, a combination of two different types of DFs is used to improve the description of the electronic structure. Specifically, the non-local Van der Waals-DF2 (VdWDF2)<sup>183,195</sup> correlation functional and the screened exact exchange DF of the HSE06<sup>189,190</sup> DF are combined. Below we will briefly discuss these DFs, first as standalone DFs and then quickly as their combination.

Local or semi-local DFs will inherently not be able to describe the longer-range electronic correlation necessary to accurately describe effects like VdW forces. Several different approaches have been developed to correct the long-range correlation of the exchange-correlation functional for such shortcomings. For instance, approaches that use a pair-wise potential based on time-dependent DFT to include VdW interaction have been developed by Grimme and coworkers<sup>185,186</sup>. Initial work of Lundqvist *et al.*<sup>182</sup>, forms the basis for multiple different VdW methods better suited for metal-molecule interactions, like the VV10<sup>187</sup>, rVV10<sup>184</sup>, VdWDF1<sup>183</sup>, and VdWDF2<sup>195</sup> DFs. Of these DFs VdWDF1 represents a truly non-empirical DF., i.e., this method is not based on fitted adjustable parameters.

In this chapter we use the VdWDF2<sup>195</sup> approach, in which a non-local (*NL*) longerrange correlation energy is added to a local (LDA) correlation energy, resulting in the following expression for the correlation functional:

$$E_C^{VdWDF2} = E_C^{LDA} + E_C^{NL,VdWDF2}$$
 (4.2).

Note that an exchange DF ( $E_x$ ) can be added to this DF that can be local, semilocal or even a non-local DF including exact exchange. The Van der Waals correction to the correlation energy can be written as

$$E_C^{NL,VdWDF2} = \int d\mathbf{r} \int d\mathbf{r}' \, \rho(\mathbf{r}) \Phi(\mathbf{r},\mathbf{r}') \rho(\mathbf{r}')$$
(4.3).

Here r is the position vector of the electron density,  $\rho(r)$  the electronic density, and  $\Phi(r,r')$  the Van der Waals kernel describing the electron density-density interactions. A full discussion of this kernel is out of scope for this chapter and the reader is referred to Refs.  $^{183,195}$  for more details.

The effects of the VdWDF2 correlation on the PES are not known *a priori*, although its addition will generally improve the description of longer-range interactions and improves over PBE in describing the adsorption of molecules on metals<sup>56,282</sup>. The presumption is that a longer-range attraction, i.e., a Van der Waals well will form in the PES<sup>126</sup>, although it is not uncommon for the middle-range interaction to become slightly more repulsive<sup>132</sup>. As the barriers for  $O_2$  on Al(111) are far away from the surface, it is expected that the use of VdW correlation will tend to reduce the barrier height<sup>124</sup>.

Moving on to the screened hybrid exchange functional, we use the HSE06<sup>190</sup> DF. This DF is very similar to the HSE03 DF<sup>189</sup>, the expression of which was later revised to obtain the HSE06 DF<sup>190</sup>. The HSE06 DF is a hybrid DF because a fraction ( $\alpha$ ) of exact (Hartree-Fock) exchange is admixed with the semi-local PBE<sup>154</sup> exchange-correlation functional according to

$$E_{XC}^{PBE0} = \alpha E_X^{HF} + (1 - \alpha) E_X^{PBE} + E_C^{PBE}$$
 (4.4).

This makes the HSE06 DF similar to the better-known PBE0<sup>153</sup> DF. However, unlike the PBE0 DF, the HSE06 DF also screens the exact exchange at longer electron-electron distances. As a result, at short distances, the DF behaves like PBE0 but at longer distances like PBE. This screening is done with a continuous and quick switching function between a long-range (*LR*) and short-range (*SR*) part in the Hartree-Fock (HF) exchange potential, such that the coulomb operator splits into:

$$\frac{1}{r_{ij}} = \underbrace{\frac{1 - \operatorname{erf}(\omega, r_{ij})}{r_{ij}}}_{SR} + \underbrace{\frac{\operatorname{erf}(\omega, r_{ij})}{r_{ij}}}_{LR}$$
(4.5),

where  $r_{ij}$  is the distance between electrons i and j,  $\operatorname{erf}(\omega, r_{ij})$  is the Gaussian error function, and  $\omega$  is the screening length parameter<sup>189,190</sup>. The result of this adaptation of the HF exchange potential is that the HSE06 exchange-correlation functional can also be partitioned into a short and long-range part, such that:

$$E_{XC}^{HSE06} = \alpha E_X^{HF,SR}(\omega) + (1 - \alpha) E_X^{PBE,SR}(\omega) + E_X^{PBE,LR}(\omega) + E_C^{PBE}$$
 (4.6)

The screening of the HF exchange for longer distances is needed to reduce computational costs<sup>189</sup>, and the screening is required to obtain a good description of the metal surface itself. Without it, the density of states of the electrons at the Fermi level would be artificially reduced<sup>158</sup>.

The implementation of the screened hybrid exchange functional in this chapter has an important difference from that of the original HSE06 DF<sup>190</sup>: In this chapter, we use a larger fraction of exact exchange. Originally, the HSE06 DF comes with a maximum exact exchange fraction  $\alpha$  of 1/4. Previous work with an HSE03-like DF used  $\alpha = 1/3^{124}$  but still resulted in overestimated sticking probabilities, suggesting that  $\alpha$  should be increased further. In this work, we therefore opted to use an exact exchange fraction  $\alpha$  of 1/2. Increasing the fraction of exact exchange is a common approach to improve the performance of the DF for gasphase barriers by increasing the barrier height<sup>139,257,283</sup>. An exact exchange fraction of 1/2 could also result in an overestimation of the barrier height<sup>283</sup>, as it did in similar work on  $O_2 + Cu(111)^{284}$ , see also Chapter 5. However, at the outset, we realised that we might need to compensate for a barrier-lowering effect by replacing the PBE correlation with the Van der Waals correlation<sup>124,126</sup>, as also discussed above, and for this, an increased fraction of exact exchange over the previously used value of 1/3 was deemed necessary.

The combination of both the screened hybrid exchange and the Van der Waals correlation DF results in the HSE06-1/2x-VdWDF2 DF

$$E_{XC}^{HSE06-VdWDF2} \tag{4.7}.$$
 
$$= \frac{1}{2} E_X^{HF,SR}(\omega) + \frac{1}{2} E_X^{PBE,SR}(\omega) + E_X^{PBE,LR}(\omega) + E_C^{VdWDF2}$$

It is expected that the HSE06-1/2x-VdWDF2 DF will adequately describe longer-range interactions and thereby result in the presence of a VdW well in the entrance channel, whilst hopefully also still correctly describing the barrier height. In the next chapter, i.e., Chapter 5, the DF defined by Equation 4.7 is presented as the first hybrid-VdW DF to yield dynamics results for the DC of  $O_2$  on Cu(111). For that system the DF tended to underestimate the reaction probability, i.e., it overestimated the barrier heights<sup>284</sup> (see also Chapter 5). Although for  $O_2$  + Cu(111) this was the first DFT result to ever underestimate sticking, we do not expect that the HSE06-1/2x-VdWDF2 would also result in an underestimated sticking probability for the  $O_2$  + Al(111) system based on the previous results obtained with  $\alpha = 1/3^{124,280}$ , and on  $O_2$  + Al(111) having only a single barrier to reaction in the entrance channel, unlike the  $O_2$  + Cu(111) system which also has a second barrier in the exit channel.

Lastly, it is important to differentiate the HSE06-1/2x-VdWDF2 DF from screened hybrid VdW DFs where the exchange part of the DF is not tailored to or made consistent with the Van der Waals correlation functional, e.g., VdW-DF2-ahbr<sup>193</sup>. The HSE06-1/2x-VdWDF2 DF does not represent a completely new screened hybrid VdW DF, as provided by the recent work of Hyldgaard and coworkers<sup>193,194</sup>. Instead, our DF is simply a combination of two established exchange and correlation DFs, as described above.

#### 4.2.2 Computational details

All DFT calculations are done with the Vienna Ab Initio Simulation Package (VASP) version 6.3.2<sup>200,258–262</sup> using the Van der Waals DFT implementation of Klimeš *et al.*<sup>285,286</sup>. In this chapter, all energies from the HSE06-1/2x-VdWDF2 DF are based on three distinct successive self-consistent-field (SCF) single-point calculations. The computational costs of converging the electronic structure energy with the HSE06-1/2x-VdWDF2 DF from scratch are high. Therefore, two pre-calculations, or "primers", have been performed to set up initial guesses for the electronic density and Kohn-Sham (KS) wavefunction. The first SCF primer uses the PBE-VdWDF2 DF, the second SCF calculation the HSE06-1/2x-VdWDF2 DF with a sparse HF integration grid, and the third and final SCF single point calculation uses a normal HF integration grid to improve accuracy.

All three SCF calculations, that is the two primers and the final SCF calculation, are spin-polarised calculations and use a 2x2 4-layer Al supercell (see the next section for the lattice details) with 15.0 Å vacuum above the slab. All three use a 10x10x1  $\Gamma$ -centred k-point grid and a cutoff energy of 400 eV. The core electrons of both Al and O are described by the projector augmented wave  $(PAW)^{199}$  method, as developed for the PBE DF. Methfessel-Paxton smearing with a width of 0.2 eV is used to improve convergence. The PBE-VdWDF2 primer uses the "conjugate" algorithm<sup>287,288</sup> with a convergence tolerance of  $10^{-9}$  eV, as done in other work<sup>280,284</sup>, see also Chapters 3 and 5. After this primer is finished, its electron density and KS-wavefunction are used for the next primer with the HSE06-1/2x-VdWDF2 DF, using the damped algorithm, as without this algorithm numeric stability is limited, and a convergence criteria of  $10^{-5}$  eV, or a limit of 240 SCF steps is used. Furthermore, the "Fast", i.e., sparse HF integration grid is

employed<sup>289</sup>. This final primer single-point calculation will, if all goes well, usually consume the bulk of the computational time. After this, another HSE06-1/2x-VdWDF2 single-point calculation is started using the previous KS-wavefunction with a normal HF integration grid to improve the accuracy of the final result. This final SCF single point is then converged to  $10^{-5}$  eV again. Converged results were obtained for all but one data point (U = 0, V = 0,  $\theta = 90^{\circ}$ ,  $\varphi = 30^{\circ}$ , Z = 4.0 Å, r = 1.175 Å), the energy of which was interpolated based on surrounding data points. Despite the use of these tricks, the computational demands for this project are still large: we have consumed upwards of 30 million CPU hours for this PES, where a single point typically takes a minimum of one week but can easily take two weeks or longer on a modern dual socket AMD EPYC 7351 32 core node, depending on the difficulty of the convergence.

#### 4.2.3 Lattice details

The Al bulk lattice has been relaxed using the HSE06-1/2x-VdWDF2 DF, using a 1x1x1 bulk supercell with 11x11x11  $\Gamma$ -centred k-points, whilst maintaining the other computational settings as described above. The lattice constant is relaxed at 4.041 Å. This is in good agreement with the experimental lattice constant of 4.032 Å $^{290}$ . The surface lattice structure was then further relaxed using a 1x1, 4-layer supercell with the bottom 2 layers frozen and 15 Å of vacuum using a 20x20x1  $\Gamma$ -centred k-point grid. This resulted in interlayer distances of  $d_{12} = 2.376$ ,  $d_{23} = 2.306$ , with  $d_{34} = 2.333$ . **Table 4.1** presents comparisons of this lattice expansion/contraction to other works, which shows that the top layer expansion is in good agreement with experimental and other theoretical work. To maintain consistency with the 2x2 unit cell the number of k-points parallel to the Al surface is halved for the PES production, see the computational details above.

**Table 4.1**: Comparing Al(111) surface layer expansion and contractions of this work with experiments and other theories.

|                 | LEED Experiments on $160  \mathrm{K}^{\mathrm{291}}$ | HSE03-1/3x <sup>124</sup> | LDA <sup>292</sup> | HSE06-1/2x-VdWDF2<br>(this work) |
|-----------------|--|---------------------------|--------------------|----------------------------------|
| d <sub>12</sub> | 1.7 % ± 0.3 %  | 1.4 %                     | 1.18 %             | 1.83 %                           |
| $d_{23}$        | 0.5 % ± 0.7 %  | -                         | -0.40 %            | -1.16 %                          |
| $d_{34}$        | -  | -                         | 0.22 %             | -                                |

#### 4.2.4 Fitting the PES

The interaction of  $O_2$  + A(111) is described with a continuous six-dimensional (6D) PES that is interpolated from the electronic structure calculations performed with the above-described HSE06-1/2x-VdWDF2 density functional. To obtain a good interpolation quality the corrugation reduction procedure (CRP)<sup>201,202</sup> is used. In this procedure, two three-dimensional (3D), or atomic. PESs are subtracted from the 6D diatomic PES. This is done to obtain a residual PES with reduced corrugation, which is easier to interpolate accurately. After this, the 3D PESs are added back to the full interpolated result. The resulting error of the CRP for predicting energies of points not part of the interpolation grid used to obtain the PES should be minor 115,130,202,280: previous work using the same  $(U, V, \theta, \phi)$  geometries and comparably fine grids in r and Z has shown an RMSE of 0.8 kJ/mol (0.2 kcal/mol) as long as interaction energies of the molecule with the metal are smaller than 4  $eV^{130}$ , with outliers usually below 3 kJ/mol<sup>115,202,280</sup>, see also Chapter 3. The CRP as implemented in this chapter is similar to that of Refs. <sup>124,263,280</sup>. However, a few distinctions will be highlighted below.

First, the atomic PES is not based on the HSE06-1/2x-VdWDF2 DF but on the PBE-VdWDF2 DF. This is done to mitigate the computational cost. Additionally, the atomic PES is based on spin unpolarised DFT, unlike the 6D molecular PES. This avoids convergence issues as the open-shell nature of an O atom results in significant noise in the DFT energies far away from the Al surface. Computing the 3D atomic PES with spin-unpolarised DFT does not affect the accuracy of the full 6D PES as subtracting the 3D atomic PESs from the full 6D PES merely serves to yield a 6D residual term with decreased corrugation and anisotropy. Adding the 3D atomic correction terms back on to the residual PES then yields the spinpolarised 6D DFT data at the points used for interpolation. Furthermore, the convergence criteria are slightly lighter than in the primer calculations, as discussed in Section 4.2.2, and are set to 10<sup>-8</sup> eV. These nuances are possible because the atomic PES does not need to be very accurate as long as it is physically reasonable, as also discussed in Refs. 124,280,284. For instance, by using the cheaper to evaluate PBE-VdWDF2 DF we ensure that the long-range interactions are described. As a result, one or two orders of magnitude in computational costs can be saved for the atomic potential. The U, V grid for this

3D atomic PES is similar to that used in earlier CRP work<sup>124,263,280</sup>, and the *Z*-Grid is an equidistant grid between -1.20 and 8.50  $\mathring{A}$  with a 0.05  $\mathring{A}$  spacing, leading to a total of 194 grid points for each of the 10 different surface sites.

Second, the 6D PES grid is not equidistant as in Ref. <sup>263</sup>. Instead a similar grid structure as in Chapters 3 and 5, and references <sup>124,280</sup> is used but extended to allow for longer-range interactions captured by the addition of the VdW-DF2 DF. Thus, this results in the grid: Z = [1.00, 1.50, 2.00, 2.25, 2.50, 2.75, 3.00, 3.25, 3.50, 3.75, 4.00, 4.25, 4.50, 4.75, 5.00] Å, and r = [1.000, 1.100, 1.150, 1.175, 1.190, 1.200, 1.225, 1.250, 1.300, 1.400, 1.500, 1.600] Å. To clarify this point further, these Z and r grids are used for each U, V,  $\theta$ , and  $\varphi$  geometry employed, and the values of the coordinates of the relevant geometries are shown in **Table 4.2**. The PES in the gas-phase is extrapolated beyond S.00 Å up to S.750 Å via a switching function to a 2D potential, similar to previous work <sup>263</sup>. This grid spacing limits the total number of required single points whilst maintaining enough details near the transition state and in the gas-phase to properly describe both the dissociative chemisorption and the Van der Waals interaction. All in all, this makes for a total of 5260 different single points used to interpolate the PES.

**Table 4.2**: The different combinations of the U, V,  $\theta$ , and  $\phi$  coordinates that are used in the grid to interpolate the PES. The U and V coordinates are shown in **Figure 4.1**.

| Site name | U   | V    | [	heta,arphi]   |
|-----------|-----|------|---|
| Тор       | 0   | 0    | [0, 0], [90, 0], [90, 30]                                     |
| Bridge    | 1/2 | 0    | [0, 0], [90, 0], [90, 60], [90, 90]                           |
| HCP       | 1/3 | 1/3  | [0, 0], [45, 30], [45, 210], [90, 0], [90, 30]                |
| TtH       | 1/6 | 1/6  | [0, 0], [45, 30], [45, 120], [45, 210], [90, 30], [90, 120]   |
| TtF       | 1/3 | -1/6 | [0, 0], [45, 150], [45, 240], [45, 330], [90, 240], [90, 330] |
| FCC       | 2/3 | -1/3 | [0, 0], [45, 150], [45, 330], [90, 0], [90, 330]              |

## 4.2.5 Quasi-classical trajectory dynamics

The continuous 6D CRP-PES can be used to compute the reaction probabilities of  $O_2$  on Al(111) with dynamics calculation using the quasi-classical trajectory (QCT) method <sup>210,211</sup>. QCT calculations include the zero-point energy of the molecule through the initial conditions imposed, after which the equations of motion are propagated classically in time<sup>210,211</sup>. The molecule is initially placed at

7.00  $\mathring{A}$  above the surface with a given incidence energy, with its velocity vector pointing along the surface normal. The trajectory is counted as reacted if the O<sub>2</sub> bond length exceeds 1.59  $\mathring{A}$ , or it is considered scattered if the molecule-surface distance exceeds 7.00  $\mathring{A}$  and the velocity of the molecule points away from the Al surface. The reaction probability is then calculated as:

$$P_r = \frac{N_r}{N_T} \tag{4.8},$$

where  $N_T$  is the total number of trajectories, and  $N_r$  the number of trajectories that reacted. See Refs.<sup>124,125,130</sup> for further details on the implementation of the QCT dynamics.

To assess the quality of the DF, computed sticking probabilities need to be compared to King and Wells experiments<sup>55,69,126</sup>. In this chapter, we compare with the supersonic molecular beam experiments of Österlund et al.<sup>224</sup>. The experimentalist varied the nozzle temperature  $(T_N)$  and used seeding in He and anti-seeding in Xe to vary the  $E_i^{\perp}$ . For the sticking curve that we aim to reproduce the authors stated that all O<sub>2</sub> molecules were in the vibrational ground state. However, no time of flight measurements are available for this study<sup>224</sup>. Moreover, previous theoretical studies used a  $T_N = 300 \ K^{124,280}$ , thus, to fairly compare the effect of the incidence energy on the DC of O2 we computed the reaction probabilities as a function of single  $E_i^{\perp}$  values with the vibrational temperature of O<sub>2</sub> taken to be the same as in the previous chapter, i.e., 300  $K^{124,280}$ . To describe the effect of the high rotational cooling of O<sub>2</sub> the rotational temperature is simply taken as having a single value of 9  $K^{264}$ ; this represents an approximation. In the QCT of this chapter, we have allowed the states v = 0 - 3and i = 1 - 49 to get occupied. This results in an 80% occupation of the rovibrational ground state: v = 0, i = 1, see Ref. <sup>130,136</sup> or Chapter 3 for more information. Note that even j states are forbidden via nuclear spin statistics for O<sub>2</sub> in the electronic ground state. The supporting information (SI) of Ref. <sup>280</sup> provides a breakdown of all the occupied initial states (or see the previous chapter Section 3.2.5.). To compute the reaction probabilities  $(P_r)$  with converged statistics we ran at least  $10^5$  trajectories per  $E_i^{\perp}$ .

#### 4.3 Results and discussion

Below the results will be discussed in three distinct sections. In the first section, the effects of the DF on the electronic structure description and potential energy surface are discussed. The second section discusses the QCT results and compares them to previous work. Lastly, the impact of the new HSE06-1/2x-VdWDF2 DF is discussed in the context of the literature and what these results mean for future descriptions of this system.

#### 4.3.1 Potential energy surface and barrier analysis

Before discussing the new QCT dynamics results, it may be insightful to discuss the effects of the VdW correlation and the increased exact exchange fraction of the HSE06-1/2x-VdWDF2 DF on the electronic structure of the  $O_2$  + Al(111) system, and the resulting changes of the PES compared to previous electronic structure calculations with  $\alpha$  = 1/3 and using PBE correlation 124,145,280.

The most immediate and important change is the consistent presence of a VdW well. This well appears in the entrance channel, i.e., at larger molecule-surface distances than where the barrier to dissociation is found, at about 3.5 Å above the Al(111) surface. In **Figure 4.2** a selection of potential curves including VdW wells are plotted as a function of the molecule-surface distance (Z) for  $O_2$  at a constant bond length r=1.19 Å. The PES cuts shown in **Figure 4.2** differ in the surface site (U, V) and  $O_2$  orientation given by  $\theta$  and  $\varphi$ . **Figure 4.2** shows that the VdW well appears to be almost completely independent of the  $O_2$  adsorption site and  $\varphi$ . However, the depth and location in Z of the well do depend on  $\theta$ . The well-depth depends on whether the molecule is orientated parallel or normal to the surface. The well tends to be shallowest and furthest away from the surface for  $O_2$  orientated normal to the surface, and deepest and closest to the surface for the planar orientation. These results are reminiscent of the VdW wells that are computed for  $O_2$  + Cu(111), see Chapter 5, with the same HSE06-1/2x-VdW DF as used here<sup>284</sup>.

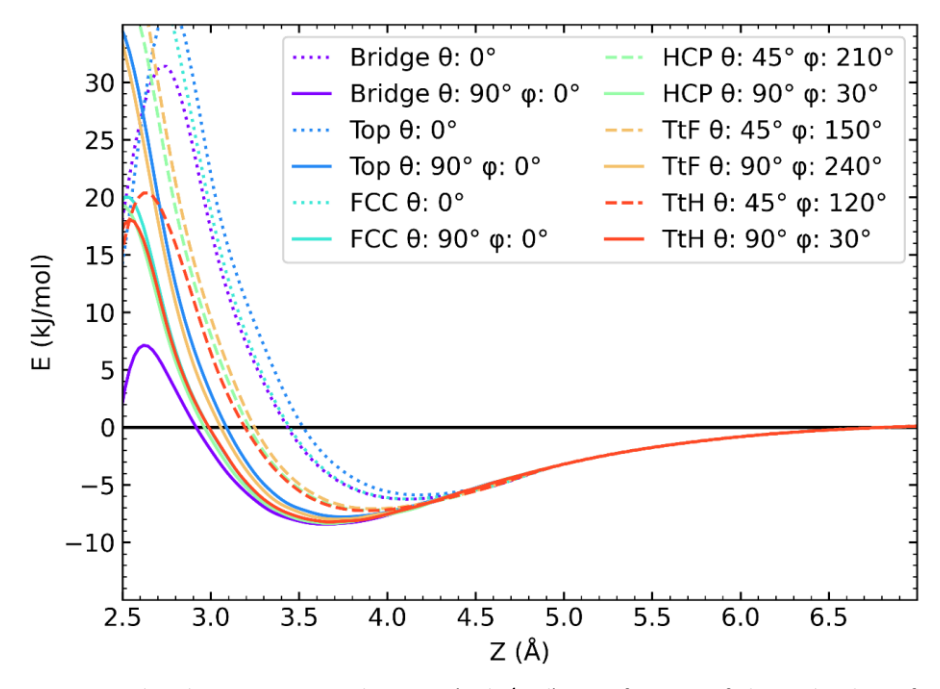


**Figure 4.2**: The electronic potential energy (in kJ/mol) as a function of the molecule surface-distance Z for a fixed  $O_2$  bond length of 1.19 Å at different U, V impact sites and for different molecular orientations (see also **Figure 4.1**).

Unlike the surface site independence of the VdW well, Figure 4.2 also shows a glimpse of a different dependence effect, i.e., a strong dependence of the barrier height on the impact site of the molecule. Although the bond length is kept constant in Figure 4.2 the results obtained at lower Z values strongly suggest that the barriers vary greatly depending on the  $O_2$  geometries. The actual barriers to dissociation occur at slightly elongated bond lengths as also found earlier  $^{280}$  in Chapter 3. The actual barrier heights are presented in Table 4.3. This table also compares with the barrier heights obtained with the HSE03-1/3x DF  $^{124}$  and the non-self-consistent field (NSCF) approach implemented through the HSE03-1/3x@RPBE DF (see Chapter 3), which amounts to obtaining the electronic energy through a single application of the HSE03-1/3x DF to a converged RPBE density  $^{280}$ . Furthermore, the left column of the table is colour-coded depending on the relative difference of barrier heights between the results of the HSE06-

1/2x-VdWDF2 DF and the HSE03-1/3x DF to aid the reader in judging the shifts in barrier heights.

**Table 4.3**: Barrier heights (in kJ/mol) computed for specific U, V, θ, φ geometries for  $O_2$  + Al(111) with the HSE06-1/2x-VdWDF2 DF, the HSE03-1/3x DF<sup>124</sup>, and the NSCF HSE03-1/3x@RPBE DF(Chapter 3)<sup>280</sup>. The colour of the barrier location tab indicates the difference between the barrier height computed with the HSE06-1/2x-VDWDF2 DF and the HSE03-1/3x DF. Red indicates a higher barrier energy for the HSE06-1/2x-VdWDF2 DF and blue a lower energy. A deeper/darker colour indicates a larger effect. Colour distinctions are made, i.e., binned per 0.5 kcal/mol (≈ 2 kJ/mol). For each DF the lowest and highest values of the barrier height computed with the DF are indicated with single and double underlining, respectively.

| Location                | HSE06-1/2x-VdWDF2 | HSE03-1/3x        | HSE03-1/3x@RPBE   |
|-------------------------|-------------------|-------------------|-------------------|
|                         | ( <i>kJ/mol</i> ) | ( <i>kJ/mol</i> ) | ( <i>kJ/mol</i> ) |
| <i>TtF θ: 0°</i>        | 26.7              | 22.9              | 29.1              |
| TtF θ: 45° φ: 150°      | 25.4              | 26.1              | 38.0              |
| TtF θ: 45° φ: 240°      | 13.4              | 12.5              | 16.7              |
| TtF θ: 45° φ: 330°      | 15.9              | 14.4              | 16.6              |
| TtF θ: 90° φ: 240°      | 26.4              | 23.6              | 28.7              |
| TtF θ: 90° φ: 330°      | 9.9               | 10.7              | 12.8              |
| <i>TtH θ: 0°</i>        | 26.1              | 21.9              | 27.7              |
| TtH θ: 45° φ: 120°      | 14.1              | 12.8              | 16.9              |
| TtH θ: 45° φ: 210°      | 24.9              | 25.3              | 36.3              |
| TtH θ: 45° φ: 30°       | 15.9              | 14.4              | 16.8              |
| TtH θ: 90° φ: 120°      | 25.8              | 23.7              | 37.9              |
| TtH θ: 90° φ: 30°       | 9.3               | 10.1              | 12.3              |
| FCC θ: 0°               | 34.4              | 26.9              | 38.5              |
| FCC θ: 45° φ: 150°      | 25.0              | 24.6              | 32.5              |
| FCC θ: 45° φ: 330°      | 39.1              | <u>39.9</u>       | <u>60.0</u>       |
| FCC θ: 90° φ: 0°        | 11.0              | 11.5              | 13.5              |
| FCC θ: 90° φ: 330°      | 12.4              | 12.4              | 14.6              |
| Bridge θ: 0°            | 23.0              | 19.5              | <i>25.5</i>       |
| Bridge θ: 90° φ: 0°     | <u>2.0</u>        | <u>4.7</u>        | <u>6.6</u>        |
| Bridge θ: 90° φ: 60°    | 21.0              | 19.6              | 29.7              |
| Bridge θ: 90° φ: 90°    | 30.7              | 29.5              | 51.4              |
| <i>HCP θ: 0°</i>        | 28.6              | 22.8              | 34.6              |
| HCP θ: 45° φ: 210°      | 23.9              | 23.3              | 31.0              |
| HCP θ: 45° φ: 30°       | <u>39.2</u>       | <u>39.9</u>       | 56.2              |
| HCP θ: 90° φ: 0°        | 9.8               | 10.4              | 12.7              |
| HCP θ: 90° φ: 30°       | 11.2              | 11.4              | 13.7              |
| <i>Top θ: 0°</i>        | 30.9              | 26.8              | 29.8              |
| <i>Top θ: 90° φ: 0°</i> | 25.4              | 22.7              | 24.4              |
| Top θ: 90° φ: 30°       | 25.2              | 22.5              | 24.4              |

The results presented in **Table 4.3** are also shown in the form of a bar plot in **Figure 4.5** in Section 4.5.1. Both **Table 4.3** and **Figure 4.5** show that the barrier

heights to DC computed with the HSE06-1/2x-VdWDF2 are not very different from the values computed with the HSE03-1/3x DF: The majority of the barrier heights are within  $\pm 1$  kcal/mol ( $\approx 4.2$  kJ/mol), of one another. This is true except for three configurations in which  $O_2$  is oriented normal to the surface and impinges on an HCP, FCC, or TtH site. The barrier heights at these geometries differ by more than 1 kcal/mol. Another noteworthy element is that the difference in barriers does not seem to follow any clear trend, i.e., some barriers are lower when computed with the HSE06-1/2x-VdWDF2 DF but most are slightly higher in energy. The overall effect is that the energy range over which the barriers are spread is increased slightly when employing the HSE06-1/2x-VdWDF2 DF, or, put differently, the energetic corrugation of the barrier is increased meaning that the barrier height varies more strongly with impact site and orientation of the molecule.

The increased energetic corrugation may result in a slight broadening of the sticking probability curve. This is what was both desired and expected from the use of the screened hybrid Van der Waals DF. However, we should note that the effect on the barriers by switching DFs is small. As discussed above, most barriers are within 1 kcal/mol of the old results and thus the effectiveness of this increased energetic corrugation may be limited. Furthermore, Table 4.3 also shows the barrier heights as computed in Chapter 3 with the NSCF HSE03-1/3x@RPBE DF<sup>280</sup>. Switching to the NSCF approach only results in higher barriers than obtained with the SCF HSE03-1/3x DF, but generally seems to increase the energetic corrugation of the barrier more than switching to the HSE06-1/2x-VdWDF2 DF does. The differences between the sticking curves computed based on the NSCF and SCF HSE03-1/3x DFs were minor<sup>280</sup> and thus, the effectiveness of increasing the barrier corrugation and anisotropy by the use of the HSE06-1/2x-VdWDF2 may be expected to be limited. This concern was also raised in the previous chapter. Thus, the effectiveness of changing to the HSE06-1/2x-VdWDF2 DF might be smaller than we had hoped for unless, e.g., the presence of the VdW well would substantially alter the nature of the dynamics.

#### 4.3.2 Quasi-classical trajectory results

The QCT dynamics calculations were performed for 491 different normal incidence energies varying from  $0.020 \, eV$  to  $1.000 \, eV$  with steps of  $0.002 \, eV$ . For every incidence energy, a total of  $10^5$  trajectories were simulated using a maximum propagation time of  $1 \, ns$ . The resulting sticking probabilities ( $S_0$ ) are presented in purple in **Figure 4.3**. The experimental  $S_0$  and the  $S_0$  computed by other theories are also presented as a comparison.

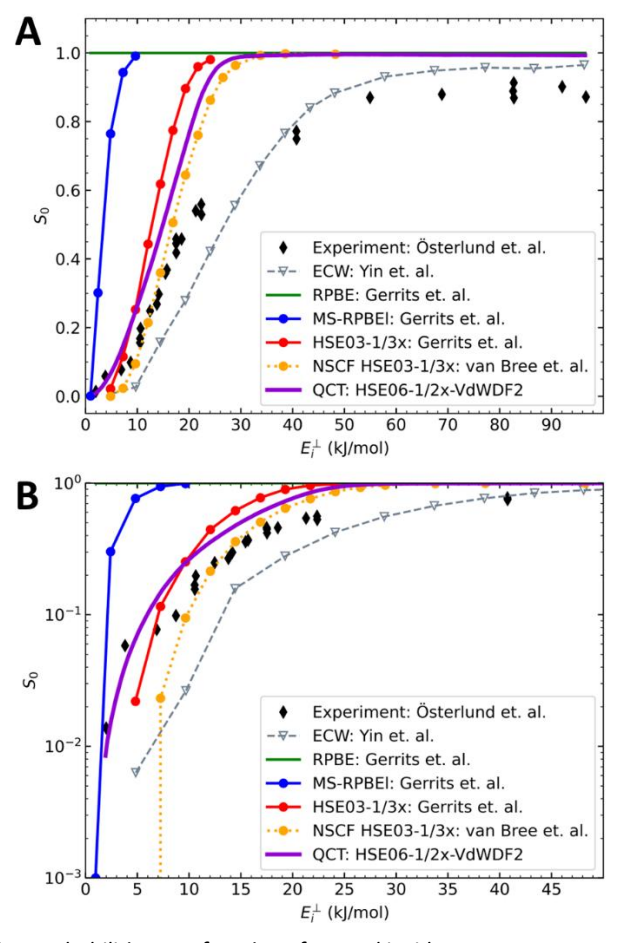


**Figure 4.3**: Sticking probabilities as a function of normal incidence energy; **A**: normal y-axis; **B**: Log y-axis, and shorter range of the x-axis, for clarity. Plotted are the sticking probabilities of the experiments (black diamonds) by Österlund et al.<sup>224</sup>, ECW results of Yin et al.<sup>230</sup>(Grey dashed line), results using the RPBE DF (green solid line), MS-RPBEI DF(blue solid line), and the HSE03-1/3x DF (red solid line) of Gerrits et al.<sup>124</sup>, the NSCF HSE03-1/3@RPBE DF (orange dotted line) of Chapter 3, and the HSE06-1/2x-VdWDF2 DF (this work, purple solid line).

The onset of  $S_0$  for the HSE06-1/2x-VdWDF2 DF is best seen in the log plot of **Figure 4.3B** and shows that some reaction already occurs at  $E_i^{\perp} = 2 \text{ kJ/mol}$ . The reactivity then quickly increases to 1 over the range of 2 - 32 kJ/mol, as seen in both **Figure 4.3A** and **Figure 4.3B**. For higher  $E_i^{\perp}$  the  $S_0$  remains constant around 1, although a maximum of 0.996 is found at  $E_i^{\perp} \approx 57 \text{ kJ/mol}$  after which  $S_0$  seems to consistently drop slowly, with a tiny amount, to 0.992 for  $E_i^{\perp} = 100 \text{ kJ/mol}$ .

The low energy threshold to the reactivity is not unexpected as the corresponding normal incidence energy of 2 kJ/mol is similar to the smallest barrier height found in Table 4.3 (see the singly underlined minimum barrier). As discussed earlier<sup>280</sup> in Chapter 3, the shape of the PES and the lack of accessible rovibrational energy for the DC of O2 means that most of the dissociation will be driven by the normal incidence energy of the molecule. Furthermore, the maximum barrier height found in **Table 4.3** is only a few *kJ/mol* higher than the value of  $E_i^{\perp}$  at which the computed sticking probability appears saturated. Unlike found for the dissociation of  $O_2$  on  $Cu(111)^{284}$  in the next chapter, the overwhelmingly greater part (by more than one order of magnitude) of the DC of O<sub>2</sub> on Al(111) occurs via a direct mechanism (Section 4.5.2. and **Figure 4.6**). The minor drop in reactivity for very high  $E_i^{\perp}$  is most likely caused by an effect similar to the bobsled effect<sup>273,293,294</sup> where the fast O<sub>2</sub> molecules barrel beyond the early barrier to hit a potential wall behind it and are forced to scatter back before the O<sub>2</sub> bond length becomes large enough for dissociation. However, it is clear that this effect is very small, and therefore not worthy of much discussion.

The QCT results based on the HSE06-1/2x-VdWDF2 DF are close to the HSE03-1/3x results of Gerrits *et al.*<sup>124</sup>. The onset of sticking obtained with the HSE06-1/2x-VdWDF2 DF occurs at somewhat lower  $E_i^{\perp}$  and the saturation of the sticking occurs at a somewhat higher energy. That is, the sticking curve undergoes a slight broadening, which is expected when looking at the increased energetic corrugation of the barriers seen in **Table 4.3** and **Figure 4.5**. Like the previous HSE03-1/3x result, the HSE06-1/2x-VdWDF2 curve represents a substantial improvement over previous GGA or mGGA-based results. The newly computed curve captures the onset of the experimentally determined  $S_0$  very well, although it is still not able to describe the  $S_0$  accurately for larger  $E_i^{\perp}$ .

## 4.3.3 Discussion and future prospects

The comparison of the quality of the different DFs is further aided by **Figure 4.4**. In this figure, the estimated energy shift of the  $S_0$  curve obtained for a specific DF from the experimental curve is plotted as a function of the  $E_i^{\perp}$  of the experimental reference. This means that for any  $E_i^{\perp}$  shown on the x-axis in **Figure 4.4**, the energy shift shown on the y-axis needs to be applied to the experimental result for that  $E_i^{\perp}$  to match the  $S_0$  values computed with the specific DF.

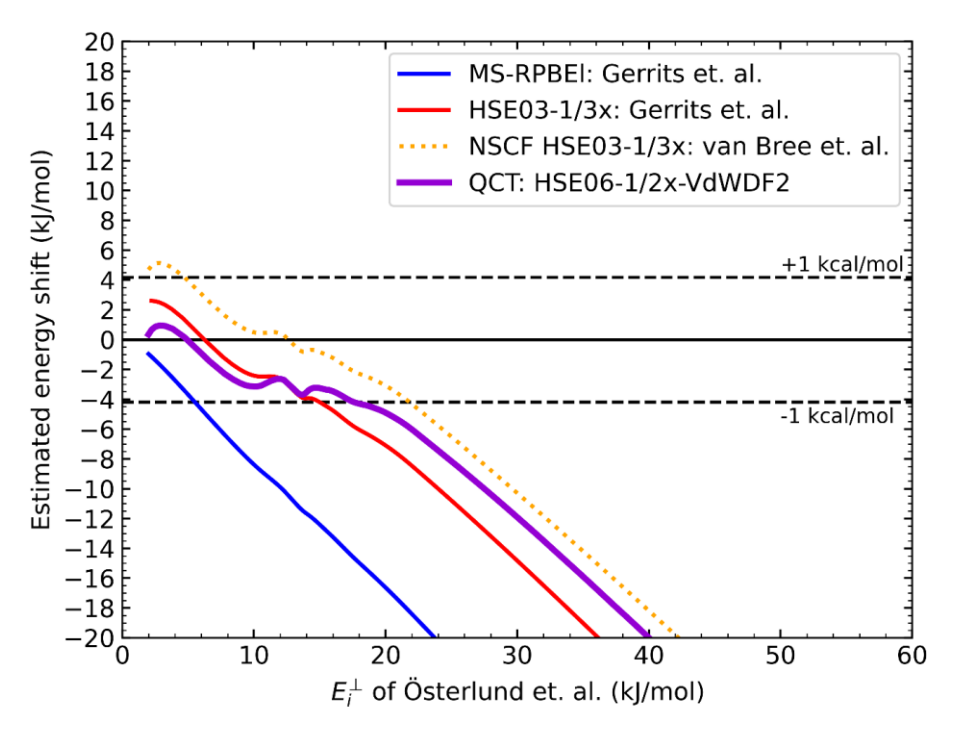


**Figure 4.4:** Estimated normal incidence energy shift (in kJ/mol) of the computed sticking probabilities relative to the experimental results of Österlund et al.<sup>224</sup> as a function of the normal incidence energy of the same experimental reference. The 1 kcal/mol boundary is indicated by dashed lines. Shown are results based on the MS-RPBEI DF (blue) of Gerrits et al.<sup>124</sup>, HSE03-1/3x DF (red) of Gerrits et al.<sup>124</sup>, the NSCF HSE03-1/3x@RPBE DF (orange dotted) of Chapter 3, and the HSE06-1/2x-VdWDF2 used here (purple). The x-axis is cut off at 60kJ/mol and energy shifts smaller than -20 kJ/mol are not plotted for clarity of the plot.

**Figure 4.4** shows very clearly that the onset of the  $S_0$  curve is described very accurately by the HSE06-1/2x-VdWDF2 DF. Even though the description of the HSE03-1/3x DF was already within chemical accuracy for the onset, the HSE06-1/2x-VdWDF2 is a better match to the experimental onset, as can also be seen

in **Figure 4.3**. However, the results depicted in **Figure 4.4** are very sobering for the impact of the combined effect of using VdW correlation and increasing the fraction of exact exchange on the 6D dynamics. The overall improvement over the HSE03-1/3x DF is limited as both DFs quickly deviate from the experimental  $S_0$  once the incidence energy in the experiments exceeds  $22 \, kJ/mol$ . It is clear that the minor broadening of the sticking curve that resulted from the implementation of the VdW correlation, although present, is not enough to lead to agreement with experiments within chemical accuracy over the entire energy range shown.

In the end, these results raise a major question for the  $O_2$  + Al(111) system: what does this mean for the ability of DFT combined with the BOSS model to accurately describe O<sub>2</sub> + Al(111)? In this chapter, we have employed one of the least reactive forms of a screened hybrid VdW DF that can be constructed based on the generic HSE06 expression. Any reduction of the fraction of exact exchange will result in more GGA-like results, thus increasing the reactivity. Using even higher mixing ratios seems doubtful as there are formal reasons for limiting the fraction of exact exchange to values equal to 1/n with n a whole number 152, and the use of n=1 would be completely replacing the semi-local exchange with exact exchange. Furthermore, the VdW-DF2 description of electron correlation remains one of the better methods to describe long-range molecule-metal interactions 126,129. Yet, the composite DF tested here with  $\alpha = 1/2$  yields only marginal improvements over the previously used screened hybrid DF with  $\alpha =$ 1/3. Lastly, the NSCF HSE03-1/3x@RPBE approach<sup>280</sup> yielded a larger energetic corrugation of the barrier than either SCF approach, yet still resulted in only small changes in the computed  $S_0$  curve relative to the SCF curve. Thus, an improvement of the computed  $S_0$  for  $O_2$  on Al(111), by any new DF, would need to come from a larger increase of the energetic corrugation of the barrier, or another large change of an aspect of the PES of which the importance is not foreseen at present. However, the similarities between the HSE06-1/2x-VdWDF2 and HSE03-1/3x barriers cast doubt on the possibility of any other screened hybrid-based DF to achieve such radical changes. Therefore, we argue that it is unlikely that the combination of screened HF exchange with VdW correlation DFs shall result in an accurate description of the  $O_2$  + Al(111) system if one also sticks to the use of the BOSS model for the dynamics.

To improve the accuracy of the theoretical description we could try to go beyond the hybrid level of DFT. However, we emphasise the already high computational demands of plane-wave screened hybrid DFT for this system and for O<sub>2</sub> + Cu(111)<sup>284</sup>, see also Chapter 5. These high costs make the brute-force use of any higher level of theory impractical at this time. This means that DFT methods like the random phase approximation (RPA) or other types of theory like Quantum Monte Carlo remain unfeasible to be used for more than the calculation of a few barrier heights. Although these types of calculations can be insightful to benchmark a select few barrier heights 114,115,249,295, such calculations will not allow for QCT dynamics to compute sticking curves. Another option to possibly improve the quality of the screened hybrid DF is to mix mGGA exchange instead of GGA exchange with exact exchange <sup>157,296</sup>. This type of mGGA-hybrid DF is still untested for molecule-metal systems. One could also try the recent DFs in which screened exchange DFs that are tailored to and are consistent with VdW-DFs combined with them<sup>193,194</sup>. However, before mapping out a completely new PES with a new DF and then testing it with dynamics calculations one might also attempt the QMC-DF approach<sup>115</sup>, in which one would try to reproduce the barrier height computed with diffusion Monte-Carlo by fitting a parameter in the generic, well-chosen, combination of a screened hybrid DF with a VdW correlation DF. For a proper description of the energetic barrier corrugation one might need to verify beforehand whether the energetic corrugation is well described with this approach of at least a few different barrier geometries.

If the construction of a PES at the screened hybrid or higher level of theory will remain as computationally expensive as in this chapter, then choosing a more advanced electronic structure method cannot be done lightly, as already explained. Thus, before trying yet another new DF or electronic structure approach to improve the description of DC of  $O_2 + Al(111)$  it may be more fruitful to briefly explore the effects and limitations of the approximations made in the BOSS model. Eliminating unfounded approximation in the BOSS model may, at this point, prove computationally less demanding than any further advancements in electronic structure calculations.

Surface temperature  $(T_5)$  effects, whether associated with surface phonons or electronic excitations in the metal, remain an unlikely cause for the disagreement with experiment, as the experiments of Österlund et al.<sup>224</sup> have shown no discernible influence of  $T_s$  on the reactivity over a  $T_s$  range of 90 - 650 $K^{224}$ . Thus, only a minor effect of surface atom displacements arising from the non-zero surface temperature in the experiments would be expected on  $S_0$ . Furthermore, the barriers to DC are generally located early in the entrance channel, i.e., at molecule-metal distances commonly larger than 2.5 Å, which also means that the perturbation of surface atom motion due to the incoming molecule may be limited<sup>274,275</sup>. This suggests a limited effect of any energy loss of the impinging molecule to surface atom motion that might occur before overcoming the barrier. As an additional test, the expected upper bound of the effect surface atom motion can be calculated using the simple, Baule model<sup>297</sup> and we show the effect in Figure 4.7 in Section 4.5.3. The Baule method treats the molecule and the surface atoms as hard spheres, and will likely result in an overestimated effect of surface atom motion. Nevertheless, Figure 4.7 does indicate that including surface atom motion may result in better agreement of the computed  $S_0$  with experiments for low incidence energies, i.e.,  $E_i^{\perp} < 26$ kJ/mol. For larger  $E_i^{\perp}$  the influence of surface atom motion will likely remain too small to result in an improved agreement with experiments. Therefore, the effect of the static surface approximation, i.e., of using an ideal and static surface in the dynamical model, may be relatively small.

If using the static surface approximation would not have a large impact, could making the Born-Oppenheimer approximation still be a cause of concern? Systems with low charge transfer energies may be more susceptible to, e.g., ehp excitation  $^{170,281,298}$ . Ehp excitation is commonly modelled by the use of electronic friction techniques  $^{299}$ , but the effect of electronic friction has not yet been modelled for the  $O_2$  + Al(111) system in conjunction with a PES obtained using a DF featuring screened exact exchange. One reason for this may be that there are two strong arguments against electronic friction having a substantial effect. First, the barrier is early, so the  $O_2$  will likely not sample higher electronic densities of the metal, thus limiting the effectiveness of electronic friction. Second, electronically adiabatic calculations on DC of  $O_2$  on Ag(111) $^{162}$ , in which reaction occurs at much higher energies than on Al(111) $^{162,224}$ , and calculations employing

the local density friction approximation (LDFA) on DC of N<sub>2</sub> on a metal surface<sup>171,300</sup> suggest that the DC of these "heavier molecule", i.e. heavier than H<sub>2</sub>, is not much affected by ehp excitation, likely due to the lower velocities exhibited by molecules heavier than H<sub>2</sub><sup>300</sup>. This might seem to suggest that ehpexcitation may also have only a small influence on reducing reactivity. There are two reasons why this preliminary conclusion might not hold. Firstly, calculations using a different electron friction model, e.g., orbital dependent friction (ODF), suggest a much larger influence of ehp excitation on DC of N<sub>2</sub> + Ru(0001) than calculations using the LDFA model<sup>171</sup>. Currently, it is not yet known which of the two electronic friction methods is best, or whether either of the two methods is accurate for modelling the effect of ehp excitation on DC on metals<sup>161</sup>. Secondly, for low  $E_{CT}$  systems, a strong electronically non-adiabatic effect can also occur through jumps of electrons between electronic states in which either the neutral molecule or the molecular anion interacts with the surface<sup>301</sup>. The non-adiabatic couplings between such states are quite strong, and modelling of the associated non-adiabaticity requires a method that is suited to deal with the associated "strong-coupling case", like the independent electron-surface hopping (IESH) method of Tully and co-workers<sup>59,302</sup>.

An argument in favour of the BOSS model is the semi-quantitative agreement achieved with experiment of sticking probabilities computed with the BOSS model using a PES calculated with the embedded correlated wavefunction (ECW) approach by Yin *et al.* who used CASPT2 for the embedded cluster<sup>230</sup> (see also **Figure 4.3**). This would seem to suggest that an accurate sticking probability curve can be computed within the BOSS dynamical model, but leaves open the questions of whether this can be done with DFT, and how accurate the ECW method employing CASPT2 for the active site actually is.

In summary, the low  $E_{CT}$  of  $O_2$  + Al(111) may still imply the presence of non-adiabatic effects in the DC of  $O_2$  on Al(111) that can, per definition, not be captured by the currently employed BOSS model. Moreover,  $O_2$  incidence energy loss, whether through ehp excitation or dissipation to surface atom motion, would be expected to have its largest effect on the reactivity in the higher incidence energy range, i.e., the energy range currently most poorly described by our current BOSS-DFT approach. For future work, it should therefore be

insightful to test the effect of allowing surface-atom motion, and of ehp excitation, if only for the purpose of elimination, before looking into further alterations of the DF used.

A computationally cheap method to model the effects of surface atom motion may be the dynamic corrugation method, previously successfully implemented for  $H_2$  + Cu(111)<sup>159</sup>. For this method, we would only need a few hundred additional DFT single-point calculations to construct the coupling potential<sup>159</sup>. Alternatively one could use a high-dimensional neural network (HDNN) approach to fit the PES<sup>303,304</sup>. The cheapest method to treat electronically nonadiabatic effects is the LDFA method<sup>281</sup>, but one should also test the ODF approach<sup>171</sup>, and possibly a recently suggested electronic friction approach called scattering potential friction<sup>161</sup>. Lastly, any future work with screened hybrid DFs will have to deal with the high computational demands. Future work could try to further reduce the amount of DFT data needed for the CRP method when building the PES, as the direct product and rigid grid now used require multiple geometries that are of limited use for fitting the dynamically relevant parts of the PES. The possibilities of a Δ-machine learning neural network approach, for example, as previously implemented for liquid H<sub>2</sub>O<sup>163</sup>, come to mind to further decrease the amount of computationally demanding calculations using a screened hybrid DF. In such an approach one might first fit a GGA-VdW potential energy surface to a large amount of points and then upgrade to a screened hybrid-VdW quality PES by fitting and using the difference of energies computed for far lesser points. To our knowledge, such an approach has not yet been tested on the DC of molecules on metal surfaces.

Finally, one may look for errors in the procedure used by the experimentalists to estimate the sticking probabilities for  $O_2$  at fixed energies. The experimentalists calculated what they called the "beam energy" from the known heat capacities of He,  $O_2$ , and Xe, which is an approximate procedure<sup>224</sup>. According to the experimentalists<sup>224</sup> the spread in the incidence energy of the beams employed, and the rotational temperature used in an experiment were estimated from earlier work<sup>305</sup>. These approximate procedures to obtain the results to which we compare here may all have led to errors. Given the important role of  $O_2$  + Al(111) as a benchmark system it might be useful if the experiments were repeated, with

time-of-flight measurements to more accurately determine the energy distributions of  $O_2$  in He-seeded and Xe anti-seeded beams and more accurate determination of their rotational and vibrational temperature than was possible before.

#### 4.4 Conclusions

The combination of a DFT approach for the electronic structure of the PES and the use of the BOSS dynamical model has thus far not been able to accurately describe the DC of  $O_2$  on Al(111). Past work has strongly suggested that this is due to the inability of the workhorse electronic structure approach in surface science, i.e., GGA-DFT, to accurately describe systems for which the charge transfer energy is below  $7 \, eV$ . Although the cause of the failure of GGA-DFT is still debated, several prior works suggest that the use of hybrid DFT leads to substantial improvement in the description of systems characterised by a low charge transfer energy. Previous work on  $O_2$  + Al(111) additionally suggested that the description of this system could be improved further by increasing the energetic corrugation of the barrier. It was believed that this could be achieved by including improved long-range, VdW-, electronic correlation while simultaneously increasing the fraction of exact exchange in the exchange-correlation DF.

To test this assumption, this chapter used the HSE06-1/2x-VdWDF2 DF. This DF is a screened hybrid DF that includes a maximum admixing of  $\alpha = 1/2$  of exact exchange and relies on the VdWDF2 electronic correlation description. To test this DF a 6D static surface PES was fitted to DFT energies for over five thousand different  $O_2 + Al(111)$  configurations, using the CRP. This PES was used to perform QCT dynamics calculations for different initial  $O_2$  conditions to compute the  $S_0$  of  $O_2$  on Al(111) as a function of  $E_i^{\perp}$ , using the BOSS dynamical model.

The use of VdWDF2 correlation and the increase of the fraction of exact exchange results in two changes in the PES relative to the previous HSE03-1/3x screened hybrid PES. Firstly, a VdW well now appears in the entrance channel of the PES. This well is generally only dependent on the angle the  $O_2$  molecule makes with the surface normal. Secondly, the reaction barriers also change. The

barriers of HSE06-1/2x-VdWDF2 in some cases shift to lower but in most cases to higher energies. This results in a slight increase of the energetic corrugation of the barrier, although the changes remain small and are smaller than the changes seen in the barriers when applying the HSE03-1/3x DF in the NSCF approach to an RPBE density, as has been done previously.

The small changes in the PES from the use of the HSE06-1/2x-VdWDF2 DF do result in some changes in the  $S_0$ . The onset of the sticking curve moves to a somewhat lower energy and the sticking curve has undergone a slight broadening, due to the increase in the energetic corrugation of the barrier. However, the changes are not very large, and the distinction between the SCF and NSCF application of a hybrid DF is more substantial. As such, even though the changes in the PES and  $S_0$  are as expected, the small magnitude of these changes means that the use of the HSE06-1/2x-VdWDF2 DF has not yet resulted in the desired degree of improvement of the description of sticking of  $O_2$  on Al(111).

Furthermore, based on the comparison of the three different DF-approaches, i.e., SCF HSE03-1/3x, NSCF HSE03-1/3x@RPBE, and HSE06-1/2x-VdWDF2, we argue that much larger changes in the PES will be required to more closely reproduce the experimental  $S_0$  with the use of the BOSS-model. The results obtained here at high computational cost signal that it is unlikely that the combined BOSS and DFT approach, as currently implemented, can be made accurate enough for the DC of  $O_2$  + Al(111).

Given the above, we suggest that future work on  $O_2$  + Al(111) would first aim at eliminating the possible influences and errors associated with the dynamical approximations inherent in the BOSS model. Addressing the effects of surface atom motion can be cost-effectively done by applying the dynamical corrugation method, while one might also use the HDNN method to obtain a PES incorporating the effect of surface atom motion. The influence of electronically non-adiabatic effects like ehp excitation can be modelled with different electron friction approaches or with a method more appropriate for strong non-adiabatic electron coupling, like the IESH method, in combination with the QCT method. Future work would also do best to try and address the mounting computational

costs associated with screened hybrid DFT or other higher-level electronic structure approaches. Finally, given the important role of the  $O_2$  + Al(111) as a benchmark system, it would be good if the experiments were to be repeated to investigate the quality of the approximate procedure used by the experimentalist to arrive at initial-rovibrational-state-selective sticking probabilities for specific single incidence energies.

## 4.5 Appendices

This chapter has three appendices. The first appendix presents a visual aid for **Table 4.3**, by plotting the barrier heights displayed in the table as a bar plot. The second appendix is a brief overview of the deconvolution of the indirect and direct reaction mechanism as simulated in the QCT calculations and shows that an indirect mechanism has a minor and negligible contribution to the total sticking probability. The third appendix briefly discusses the Baule model to molecule-metal surface energy transfer and presents a figure showing an expected lower bound for the reactivity of the  $O_2 + Al(111)$  system if energy transfer to the Al surface phonons were to be included.

## 4.5.1 Reaction barrier bar-plot

The barriers to dissociative chemisorption as presented in **Table 4.3** of the main text are shown in a bar plot in **Figure 4.5** as an additional visual aid to understanding the differences in energetic corrugation of the barrier. Also plotted are the reaction barriers based on the SCF HSE03-1/3x DF of Gerrits *et al.*<sup>124</sup> and the NSCF HSE03-1/3x@RPBE DF of Chapter 3. **Figure 4.5** shows that some barriers described by the HSE06-1/2x-VdWDF2 DF are lower than those of the HSE03-1/3x DF, but most others are higher. Furthermore, **Figure 4.5** shows that there are no clear patterns based on surface site or O<sub>2</sub> geometry as to the screened hybrid VdW DF resulting in either a lower or higher barrier energy. Lastly, the NSCF results are also presented. The NSCF DF inadvertently but considerably increased the energetic corrugation of the barrier<sup>280</sup> and can thus also function as a useful DF for assessing the effect of the energetic corrugation on the sticking.

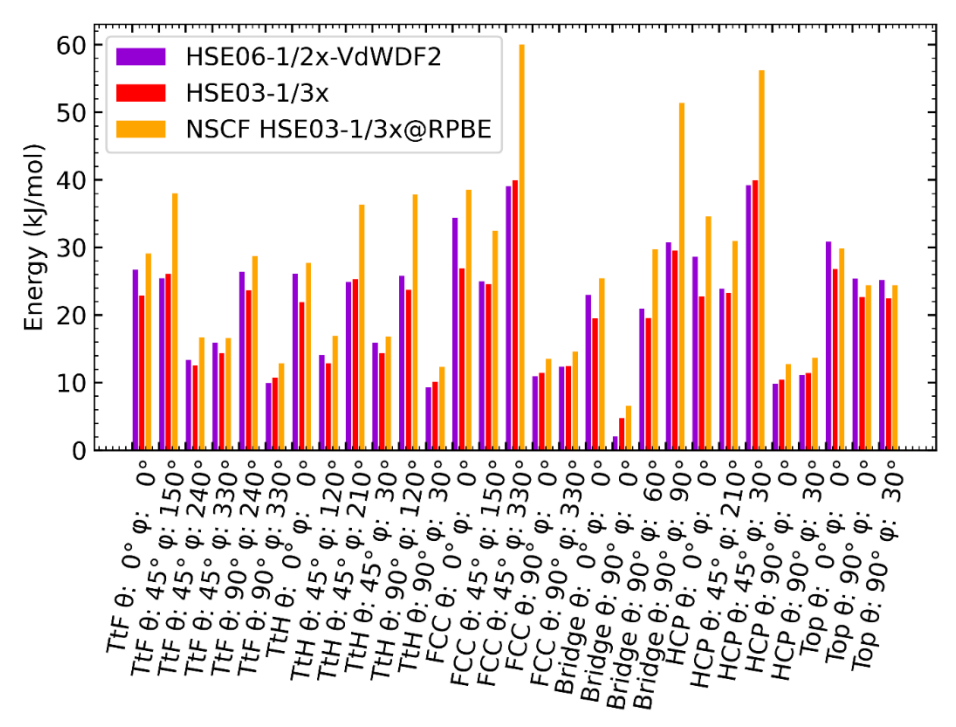


**Figure 4.5**: Barplot comparing barrier heights for twenty-nine different  $O_2$  + Al(111) geometries computed with the HSE06-1/2x-VdWDF2 DF (purple), HSE03-1/3x DF (red) as adapted from the work of Gerrits et al.<sup>124</sup>, and the non-self-consistent field HSE03-1/3x@RPBE DF (orange) as taken from Chapter 3.

## 4.5.2 Direct and indirect dissociative chemisorption

The reaction probability of  $O_2$  on Al(111) can be divided into contributions of different types of events in a similar way as was done for  $O_2 + Cu(111)$  in previous work<sup>284</sup>, i.e. Chapter 5. In short, the total reaction probability is the sum of both the direct and the indirect reaction probability where the sticking probability is the sum of the total reaction probability and the trapping probability:

$$S_0 = 1 - P_S = P_r^T + P_t = P_r^D + P_r^I + P_t$$
 (4.9).

Here  $P_s$  is the scattering probability. Any probability of a specific event is computed analogously to Equation 8 of the main text, and the conditions for reaction and scattering are described in Section 4.2.5 of the main text. Furthermore, a molecule is considered trapped if it has neither scattered nor reacted after the limit of  $1 \, ns$  propagation time has been reached. The reaction

probability is considered indirect if the molecule makes more than one "bounce" on the surface. A bounce is defined by a sign change in the momentum vector of the COM of the  $O_2$  molecule along the surface normal. For more details, the reader is referred to Chapter 5.

If the  $S_0$  shown in **Figure 4.3** of the main text is divided into the probabilities of the separate sticking events as described by Equation 4.9 then this results in **Figure 4.6**. From this figure, it is immediately clear that no trapping of  $O_2$  on the Al(111) surface occurs within the time limit we use, i.e., 1 ns. That is, all  $O_2$  molecules will either scatter or react within this timeframe. Furthermore, the contribution of indirect reaction is minimal, i.e., always one order of magnitude smaller than the contribution of direct dissociative chemisorption. The influence of the indirect mechanism is thus small although not entirely negligible.

Moreover, the indirect mechanism only occurs in an  $E_i^\perp$  regime where the  $E_i^\perp$  can be either higher or lower than an encountered reaction barrier, i.e., within the barrier energy range, see also **Table 4.3** or **Figure 4.5**. As such, one can assume that the indirect mechanism occurs via the  $O_2$  molecule impinging the surface at a geometry for which the barrier is slightly too high, with the initial collision leading to, e.g., enhanced molecular rotational motion, which leads to temporary adsorption if not enough energy is left in translational motion normal to the surface for the molecule to escape to the gas-phase. Once the molecule returns to the surface it may find a more favourable geometry for reaction, but since it has experienced at least one bounce with the Al(111) surface the reactive event will be classified as indirect.

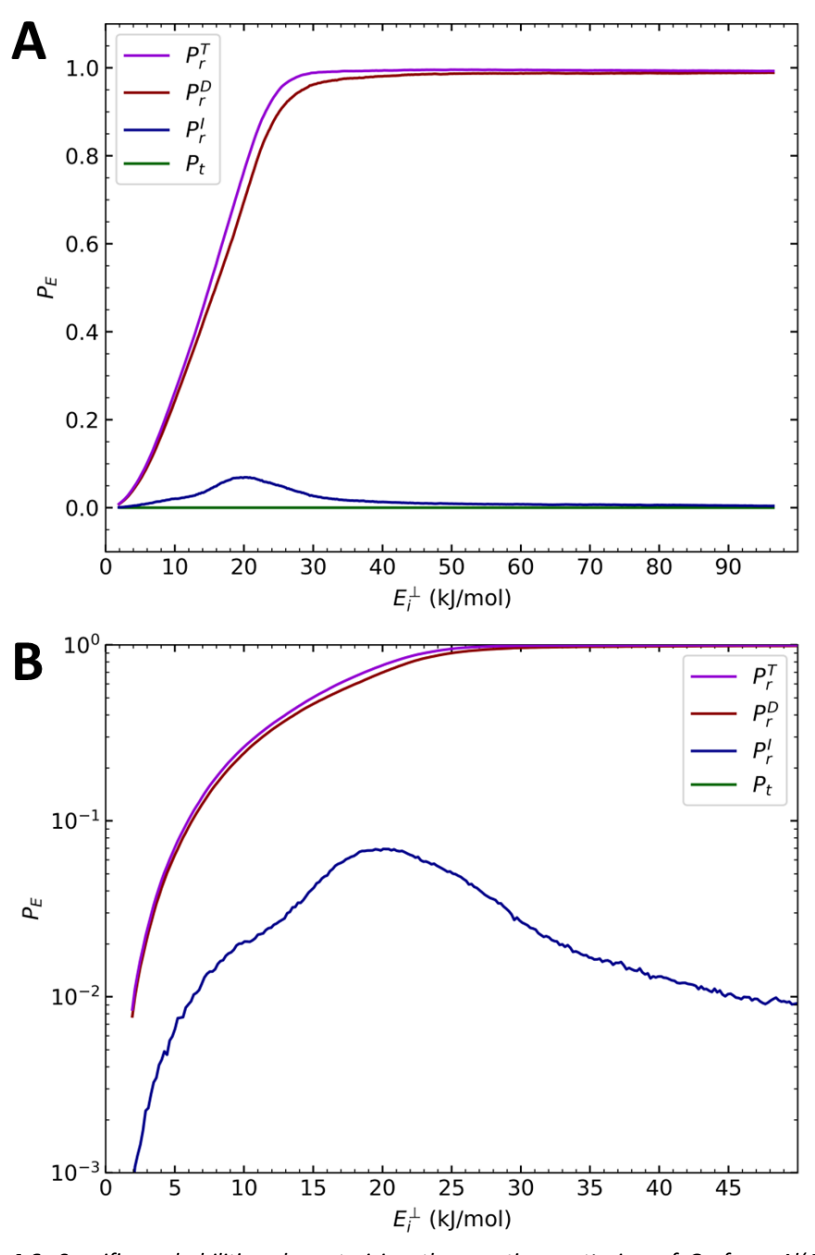


**Figure 4.6**: Specific probabilities characterising the reactive scattering of  $O_2$  from Al(111) as computed by quasi-classical trajectory calculations using the HSE06-1/2x-VdWDF2 PES. The probabilities are plotted as a function of normal incidence energy ( $E_r^{\perp}$ ), and plotted are the total reaction probability ( $P_t^{\text{T}}$ ), the direct reaction probability ( $P_t^{\text{D}}$ ), the indirect probability ( $P_t^{\text{D}}$ ) and the trapping probability ( $P_t^{\text{D}}$ ). For definitions of each type of event see the text and Ref. <sup>284</sup> or Chapter 5.

#### 4.5.3 Baule model

An expected upper bound of energy transfer between  $O_2$  and an Al surface atom can be estimated using the Baule model<sup>297</sup>, along similar lines as done in the work of Nattino *et al.* to estimate the effect of allowing surface atom motion on the inelastic scattering of  $N_2$  from W(110)<sup>131</sup>. The energy transfer in the Baule model can be computed as

$$\Delta E = \frac{4\mu}{(1+\mu)^2} E_I \tag{4.10}$$

with

$$\mu = \frac{2 * 15.999 \, u}{26.982 \, u} = 1.1859 \tag{4.11}$$

thus,

$$\Delta E = \frac{4 * 1.1859}{(1 + 1.1859)^2} E_I = 0.992 E_I \tag{4.12}.$$

We estimate that for sticking only half the total energy transfer occurs before the barrier is crossed, as only "half" a collision occurs before the system "decides" that sticking occurred. The estimated shift of  $S_0$  of **Figure 4.3** can then be estimated by shifting the  $S_0$  through changing its argument  $E_i^{\perp}$  as follows:

$$E_I^{\perp} + \frac{1}{2} \Delta E = (1 + \frac{0.992}{2}) E_I^{\perp}$$
 (4.13).

The sticking probability shifted in this way, along with the experimental and original QCT-based  $S_0$  is presented in **Figure 4.7**. This figure shows that we may still expect a non-trivial drop in  $S_0$  if the motion of surface atoms is included in future models. However, we note that the Baule model is simplistic and may well overestimate the energy transfer to surface atom motion, as was also previously shown for the scattering of  $N_2$  from  $W(110)^{131}$ . Furthermore, the barriers to reaction for  $O_2 + Al(111)$  are so early in the entrance channel that the barriers tend to be encountered before a "hard-sphere-like" collision of the molecule and the surface atoms actually can take place as the Baule model would imply. Thus, it is more likely that any future  $S_0$  computed with the inclusion of the effects of surface atom motion will end up somewhere between the QCT results of the current chapter and the lower bound as calculated with the Baule model. This area is indicated as the grey area in **Figure 4.7**.

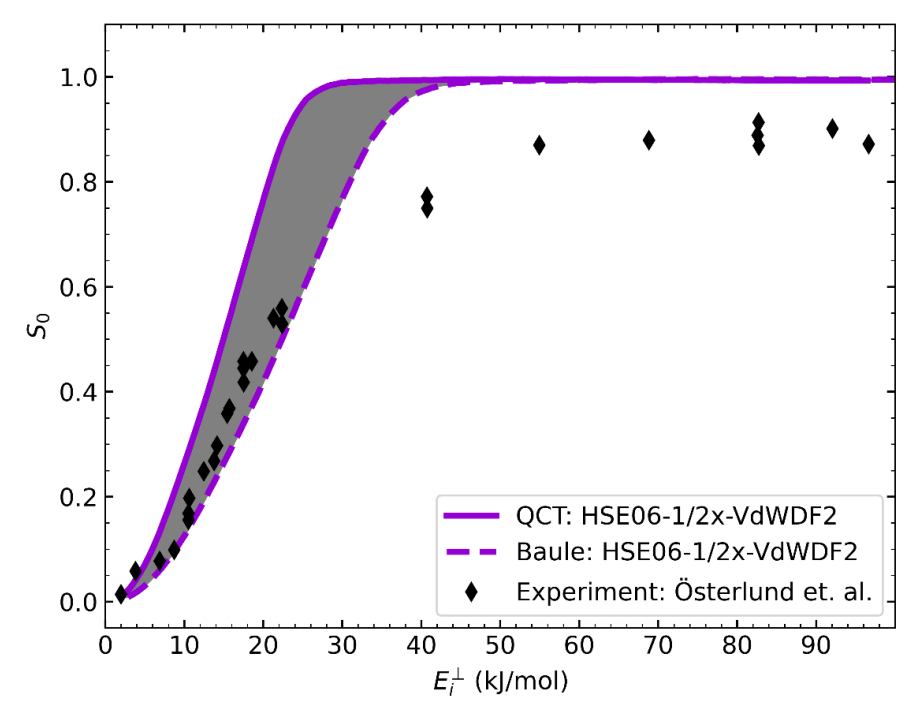


**Figure 4.7**: Sticking probabilities as a function of normal incidence energy. Plotted are the sticking probabilities measured in the experiments (black diamonds) by Österlund et al.<sup>224</sup>, as computed with the HSE06-1/2x-VdWDF2 DF using the static surface model (purple solid line), ), and as estimated from the latter by taking into account energy transfer to surface atom motion as calculated by the Baule model (purple dashed line). The grey shaded area estimates future computational results including the effects of surface atom motion.

Application of the Baule model shows that, with the use of the HSE06-1/2x-VdWDF2 DF and quasi-classical dynamics for molecular motion, the addition of surface atom motion to the model may result in substantially better agreement with experiment for incidence energies up to about  $E_i^{\perp} = 26 \text{ kJ/mol}$ . However, based on these results it seems that surface atom motion will be an unlikely candidate to improve agreement much for any higher  $E_i^{\perp}$ .